POLITECNICO DI TORINO
Repository ISTITUZIONALE

Assessment of a 1-D diesel engine model for accurate response in transient simulations

Original
Assessment of a 1-D diesel engine model for accurate response in transient simulations / Finesso, R., Marello, O., Ventura, L.. - In: INTERNATIONAL JOURNAL OF ENGINE RESEARCH. - ISSN 1468-0874. - STAMPA. - 25:10(2024), pp. 1879-1897. [10.1177/14680874241256024]

Availability:
This version is available at: 11583/2992581 since: 2024-11-20T10:39:06Z

Publisher:
SAGE Publications Ltd

Published
DOI:10.1177/14680874241256024

Terms of use:

This article is made available under terms and conditions as specified in the corresponding bibliographic description in the repository

Publisher copyright
Sage postprint/Author's Accepted Manuscript

Finesso, R.; Marello, O.; Ventura, L., Assessment of a 1-D diesel engine model for accurate response in transient simulations, accepted for publication in INTERNATIONAL JOURNAL OF ENGINE RESEARCH (25 10) pp. 1879-1897. © 2024 (Copyright Holder). DOI:10.1177/14680874241256024

(Article begins on next page)

19 November 2026

Assessment of a 1-D Diesel Engine Model for Accurate Response in Transient Simulations

Roberto Finesso*, Omar Marello, Loris Ventura
Department of Energy, Politecnico di Torino, Corso Duca degli Abruzzi 24, 10129, Torino, Italy;

*Corresponding author: roberto.finesso@polito.it; Tel.: +39-011-090-4493

Funding: This research received no external funding

Conflicts of Interest: The authors declare no conflict of interest.

Assessment of a 1-D Diesel Engine Model for Accurate Response in Transient Simulations

Abstract

The complexity of modern powertrains with their embedded control systems has increased in the last years, due to the tightening of emission regulations. Therefore, virtual calibration and Model-in-the-Loop testing can provide a great support for their preliminary assessment, in order to reduce the experimental effort. To this purpose, highly accurate engine models are required, not only at steady-state conditions, but also in transient operation. The present paper addresses the assessment and validation of a fast-running 1-D model of a diesel engine for heavy-duty applications, focusing on the transient response. In particular, a baseline model with satisfactory accuracy at steady-state operation, but not in transient conditions, is analysed and assessed with the aim of reproducing the true dynamic response of the real engine installed at the test bench, as well as the behaviour of the embedded air-path controllers. The entire methodology for the model assessment is presented step by step, and common challenges and potential pitfalls that researchers may encounter when calibrating simulation models are discussed. Finally, the impact of the test bench layout on the engine dynamic response is also evaluated and discussed.

Keywords
internal combustion engine, control algorithm, modeling, transient response, diesel engine

Introduction

As environmental awareness grows, emission limit legislation becomes increasingly more severe. To comply with these regulations the research on internal combustion engines introduced alternative combustion modes [1] and fuels [2,3] as well as technological solutions to improve the actual combustion [4–6]. The combustion was not the only area of development, as there were also innovations on the hardware and software sides. Examples of these are represented by the innovative control systems that have been introduced over the years for the air path [7] combustion [8–11] and overall management [12]

Furthermore, the growing trend in the adoption of hybrid electric vehicles (HEVs) has led to new challenges in terms of engine calibration and control, since the engine operation in a hybrid framework is very different than in conventional use.

These and future alternatives could require significant changes to the current hardware and control layout with their calibration methods. To evaluate a technology or optimize the steady-state calibration maps embedded in Electronic Control Unit (ECU), extensive testing has to be performed at the testbed [13]. However, these procedures are time consuming and expensive. Thus, in recent years, models to conduct virtual experiments have increasingly claimed considerable attention and headlines in the ICE-centered conferences and journals [14–16].

Simulation models have therefore become an essential tool for the development of modern engineering systems replicating the behaviour of real-world systems and phenomenon under different conditions. These models are designed to imitate the working of a system by considering its various components and the interactions between them. Simulation models can help researchers and engineers to identify potential problems or inefficiencies in a system, test different solutions to address them and assess and/or optimize management strategies and control systems, by means of the Model-in-the-Loop (MiL) technique, identifying a preliminary setup that will allow to achieve a desired outcome with limited experimental time [17–19]. One of the key advantages of using simulation models is their ability to allow for experimentation without incurring the risks and costs associated with real-world testing. The recent increase of computational performance and development of advanced simulation tools have greatly expanded the capabilities of models allowing their use even in real-time embedded platform [20,21].

The complexity of the models that have been applied to the ICEs varies according to their purpose. They may vary in the input and output variables, the structure, and adopted mathematical description. Commonly, two families of models can be distinguished, physics-based and black-box. The first family adopts fundamental equations such as conservation of mass and energy[22]. Black-box models are derived from observed data through system identification [23]

Among the first group, the approximation in the phenomenon description leads to three different categories: 1)3-Dimensional (3-D) Computational Fluid Dynamics (CFD), 2) 1-D CFD and 3) mean value models or 0-D. The first class exploits the equations governing fluid motion and it can describe the fluid dynamics over the three spatial dimensions. In this case, the balance is shifted towards accuracy at the expense of computation time that is high, therefore they are not used for the simulation of the whole engine but only for analysing specific subsystems. Restraining the spatial dimension to consider generally only the length, 1-D CFD models are obtained. This allows to significantly reduce computational time while maintaining an overall good accuracy. Due to this property, 1-D modeling has become a fundamental tool in ICE development with various commercial software such as GT-SUITE, which allow to simulate the entire engine. For this reason, these models are particularly suited for the assessment and development of

new control systems, by means of the MiL technique. Finally, mean value or 0-D models are obtained by neglecting the simulation of the cyclic variation of the ICE cycle and by lumping the parameters. In this case, the computational time is significantly reduced since no spatial resolution is resolved, often reaching real-time conditions [10,21]. These modes are generally adopted to realize model-base real-time algorithms, as can be seen in [9].

The second family, black-box, describes the input-output relation of a system exploiting collected data. The parameters of these models serve to map only the inputs to the outputs without having any physical meaning in terms of equivalence to process parameters. Artificial neural networks and support vector machines are examples of these kind of model that are also vastly exploited in the ICE field [24,25]. Nonetheless, to ensure accuracy and reliability, it is necessary to assess and validate the virtual model over the actual plant through a rigorous and methodological procedure. In this process, the boundary conditions and assumptions made to derive the model have to be kept in mind, since they will define the region where the model can be used [26].

On the basis of the previous background, it is clear that the development of reliable engine models, which are capable of reproducing not only the steady-state performance, but also the transient performance (including that of the embedded controllers) in an accurate way, is of fundamental importance for preliminary engine assessment through virtual calibration, but also for preliminary development and testing of new control systems through MiL.

The main objective of this paper is to present a systematic methodology for assessing the performance of a 1-D model of a diesel engine for heavy-duty applications, realized in the GT-SUITE environment, in transient operation, with the aim of reproducing the actual dynamic response of the real engine, including its air-path controllers. This involves various steps, which are described in detail in the following sections. To the authors' knowledge, there is a lack, in the literature, of studies which show detailed methodologies for assessing 1-D engine models in order to reproduce the actual dynamic performance in an accurate way. Another aspect that is discussed in the paper, is the analysis of the impact of the layout of the experimental test bench, concerning the intake engine side, on the engine transient performance. It was verified that this impact is not negligible, and this should be taken into account when designing the bench setup. We also discuss common challenges and potential pitfalls that researchers and practitioners may encounter when calibrating simulation models.

In the following, the *Experimental setup* section describes the engine, the test bench setup and the experimental tests used in the work; the *Baseline engine model* section reports a description of the initial baseline engine model that was used as a starting point in this study, the *Methodology* section presents the workflow that was followed in the model development; the *Results and discussion* section reports the results obtained by comparing the simulations with the experimental data and finally, the *Conclusions* section provides a summary of the work including the major findings.

Experimental setup

Engine

The engine considered in this work is a 3-litre EURO VI diesel one, which was modelled in GT-SUITE environment. It is endowed with short route EGR, VGT, exhaust flap, intercooler and EGR cooler. The exhaust flap is mainly used to increase the amount of recirculated gas, primarily at low loads whenever the pressure differential across the EGR valve is not sufficient to achieve the desired amount of recirculation The main specifications of the engine are reported in Table 1 while the engine layout is shown in Figure 1.

Table 1. Engine Main Specifications.

Engine type	EURO VI diesel engine
Number of cylinders	4
Displacement	2998 cc
Bore x stroke	95.8 x 104 mm
Rod length	160 mm
Compression ratio	17.5 : 1
Valves per cylinder	4
Turbocharger	VGT type
Fuel injection system	High pressure common rail

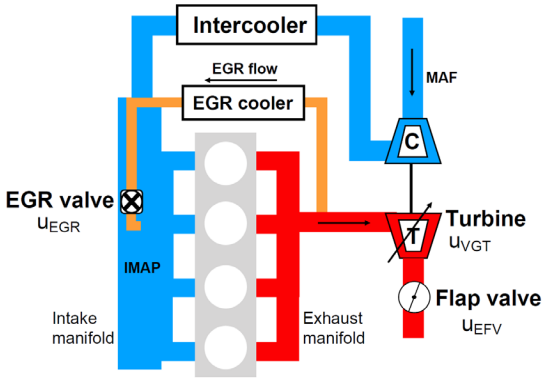


Figure 1. Engine layout.

The tested engine was instrumented with piezoresistive pressure transducers and thermocouples to measure the pressure and temperature at different locations, such as upstream and downstream the compressor, the turbine and intercooler, in the intake manifold and in the EGR circuit. Thermocouples were also used to measure the temperatures in each intake and exhaust runners. KISTLER 6058A high-frequency piezoelectric transducers were fitted to the glow-plug seat to measure the in-cylinder pressure time-histories. The dynamic testbench is at the Internal Combustion Engines Advanced Laboratory of the Politecnico di Torino. Its hardware includes a cradle-mounted AVL APA 100 dynamometer, an AVL KMA 4000 system (for continuous fuel consumption measurement), an AVL AMA i60 system (for raw gaseous emissions' measurement), an AVL 415S smokemeter (for steady-state tests). The AVL AMA i60 system simultaneously measures, at both the intake and exhaust sides, HC, NOx/NO, CO/CO_2 and O_2 by means of two complete analyser lines. PUMA Open 2 and Indicom software control the measurement devices [9].

Test description

The tests that were used in this paper for the discussion include steady-state and transient operating conditions and are described hereafter.

The steady-state tests feature 413 experimental measurements that include an engine map (126 points), an oxygen trade off on 5 different k-points (162 points), achieved varying the EGR and VGT positions and a DOE (125 points) of SOI of the main pulse and rail pressure.

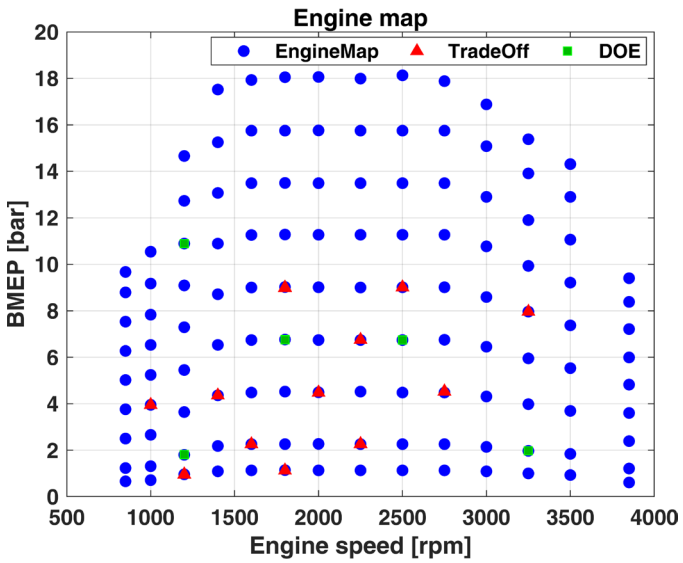


Figure 2. Engine map with tests k-points.

Various transient tests were used to assess the model transient performance but for sake of brevity only a ramp and the World Harmonized Transient Cycle (WHTC) are reported. The ramp (that from now on will be referred as 'speed/load ramp'), is a speed and load ramp in which the speed and load have been varied independently and in combination with rates of (10s, 5s, and 3s). Figure 3 represents the speed and load variation for 5s ramping time.

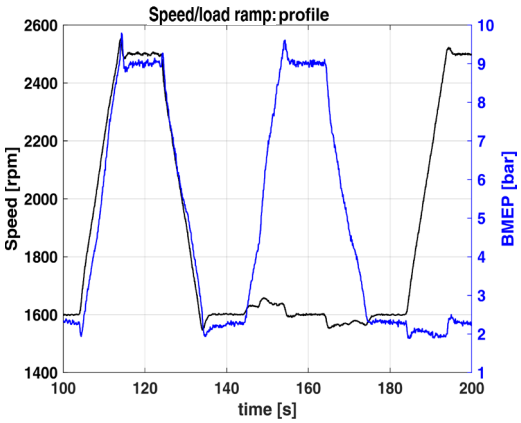


Figure 3. Profile of the speed/load ramp.

Regarding the WHTC cycle, torque and speed profile are not reported since they are commonly known. Due to the length and aggressiveness of the WHTC only a couple of sections of the entire cycle are reported in the results and discussion section, as well as cumulative plot of meaningful quantities.

The transients tests were realized by setting an engine speed setpoint for the dynamometer controller, and a torque setpoint for the test bed engine load controller, which acted on the pedal position to achieve the desired torque target.

Baseline engine model

The baseline model, which was built in GT-SIUTE environment, had been developed as a support tool for previous research activities carried out on the same engine (e.g., refer to [10]). However, a detailed investigation and assessment of its performance in transient operation was not conducted before, as it was mainly used to simulate steady-state conditions. Figure 4 reports a scheme of the model, in which the most significant subsystems are highlighted.

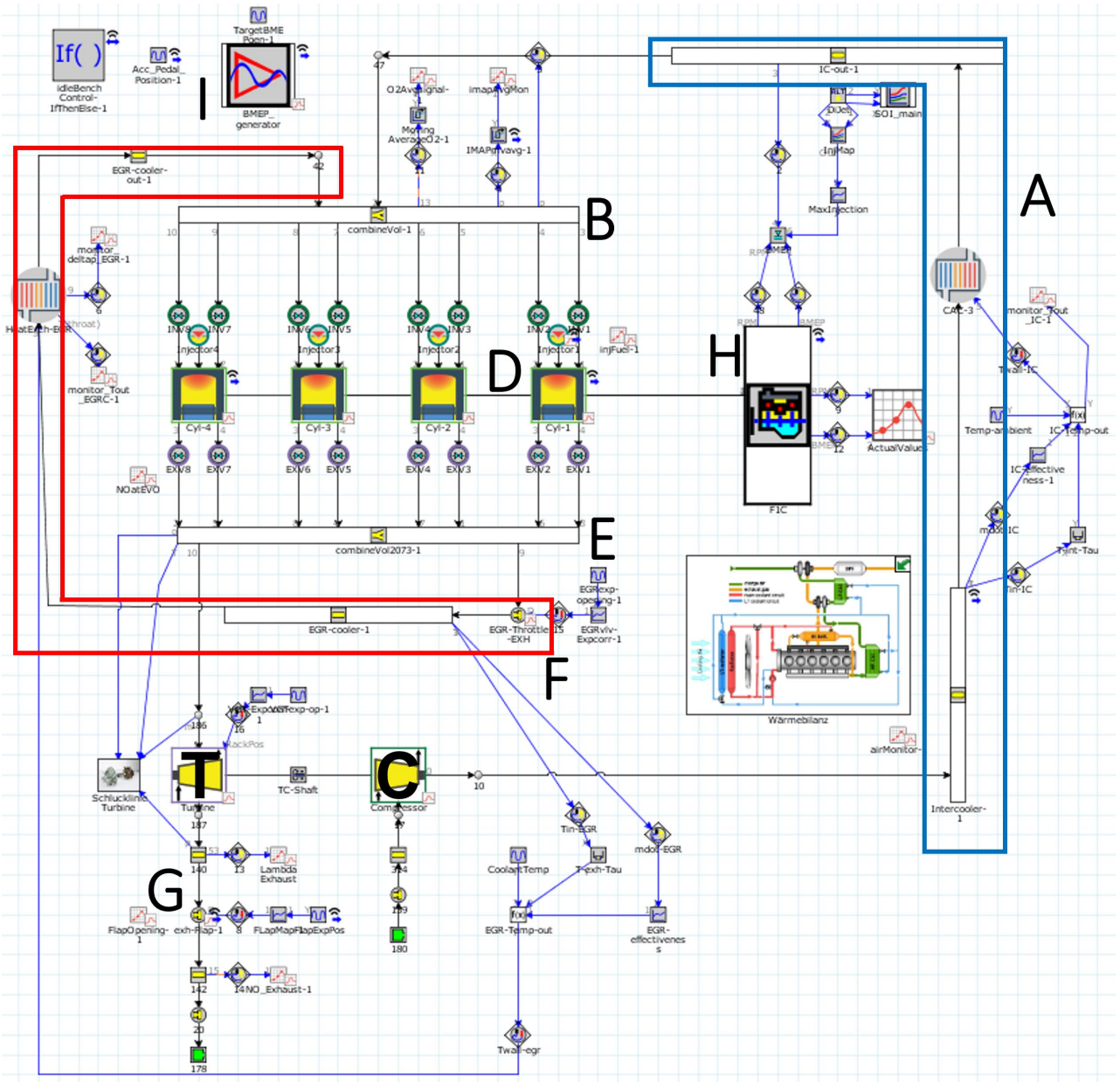


Figure 4. Scheme of the baseline engine model realized in GT-SUITE. A) Intake branch; B) Intake manifold; C) Compressor; D) Cylinder; E) Exhaust manifold; F) EGR branch; G) Exhaust flap; H) Cranktrain; I) Pedal interpretation; T) VGT.

In the figure, the following blocks are highlighted: block 'A' (intake branch), block B (intake manifold), block C (compressor), block D (cylinders), block E (exhaust manifold), block F (EGR branch), block G (Exhaust Flap), block H (cranktrain), block I (Pedal map) and block T (VGT).

The baseline model includes two PID controllers, which act on the EGR valve and on the VGT rack position, respectively. The EGR controller regulates the EGR valve diameter to match the EGR fraction target, while the VGT controller regulates the turbine rack position to match the intake manifold pressure (IMAP) target. The EGR fraction targets and IMAP targets were defined on the basis of the experimental measurements on the real engine installed at the test bench.

It should be pointed out that the EGR controller is significantly different with respect to that implemented in the real engine. In fact, the latter decides a percentage opening position of the EGR valve, in order to achieve a desired target of air mass flow.

As far as the exhaust flap is concerned, a dedicated controller was not implemented in the engine model, therefore its opening position is set directly. The main difference between the model and the real engine consists of the actuation command: the valve diameter is used as a control variable in the model, while the percentage opening position is set in the real engine.

In all simulations, the engine speed and accelerator pedal position were given to the model as input, in order to reproduce the actual behaviour of the engine installed at the test bench. The accelerator pedal position was in fact the same as that actuated in the real engine during the tests. It should also

be noted that the model includes several calibration maps which, on the basis of the speed and pedal position, define the setpoints for all the control variables of the engine (fuel quantity and start of injection for all the injection pulses, rail pressure, etc…).

Methodology

This section presents the methodology that was followed to assess the engine model in order to obtain a correct reproduction of the actual transient response measured at the test bench. Contrarily to steady-state conditions, during transient operation the engine dynamic response is affected to a great extent by the interaction between the ICE subsystems and its controllers. Therefore, an accurate reproduction of the true engine dynamic response requires on the one hand a correct modelling of the physical response of the engine subsystems (e.g., pipes, turbocharger, …) and, on the other hand, a correct reproduction of the behaviour of the real engine controllers.

The starting point for the activity presented in this paper is the baseline engine model described in the previous section, which was found to be accurate at steady-state operation, but less precise in reproducing the response of the real engine in transient operation.

The first step was the decoupling of the EGR and VGT controllers embedded in the engine model from the physical response of the engine subsystems. Therefore, the controllers were initially removed from the model, and the EGR valve and VGT rack, along with the exhaust flap, were actuated with the experimental signal profiles that were recorded during the experimental bench tests. This made it necessary to map the EGR/exhaust flap valves and the VGT rack under steady-state conditions, and to build correlations between the experimental actuation signals (expressed in opening percentages) and the control variables used in the engine model.

After implementing the previous correlations in the model, stationary and transient simulations were performed by setting the experimental actuation commands as inputs for the EGR valve, VGT rack and exhaust flap. In this way, it was possible to verify the physical response of the individual subsystems (e.g., circuits, air path, combustion, turbocharger, …) without the influence of the EGR/VGT controllers.

This step was useful to analyse and correct the mismatches which emerged. In particular, a mismatch was found between the actual inlet circuit of the test-bench and the modelled one. It was found that this mismatch had a significant impact on the engine transient response, and therefore a correction of the geometry of the inlet engine was done.

Subsequently, we moved on to the air-path controllers. In this stage we used the refined engine model to design new control systems which were able to replicate the experimental actuation signals generated by the real controllers embedded in the engine control unit (ECU). To this aim, it was necessary to define the same targets that were used in the ECU. With this approach, the developed control systems implicitly reproduced the limits and the response of the real actuators as well as the command action itself.

Once the tuning of the new control system was completed, they were integrated in the engine model, and its performance was assessed and verified through the simulation of various transient tests, i.e., the speed/load ramp and the WHTC.

Results and discussion

Evaluation of the performance of the baseline engine model

A preliminary verification of the performance of the initial baseline engine model was carried out at both steady state and transient conditions. The results of the validation process for the variables of major interest are reported in Table 2. The results were found to be satisfactory as can be seen from the values of the indices of correlation, R2, and Root Mean Square Error (RMSE).

Table 2. Validation, at steady-state conditions, of the initial baseline model – The R2 and RMSE values were obtained by comparing the simulated and experimental results.

	R2	RMSE
BMEP	0.998	0.207 bar
Torque	0.998	4.93 Nm
IMEP360	0.999	0.226 bar
EMAP	0.991	0.068 bar
IMAP (controlled)	1	0.008 bar
Lambda	0.995	0.09
Xr (controlled)	1	0.065 % (abs)
PFP	0.992	3.43 bar
Air mass flow	0.997	1.78 g/s
EGR	0.996	0.387 g/s
O2	0.986	0.184 % (abs)
NOx	0.869	84.8 ppm

On the contrary, the response of the model in transient conditions was unsatisfactory. As can be seen in Figure 5a, the teal line, that represents the simulated air mass flow into the engine over a portion of the WHTC, is very different with respect to the actual one (red line), obtained during the experimental tests. Another interesting fact is that both the simulated and actual trends of the air mass flow are quite different with respect to the target air mass (grey line) which derives from the engine calibration desired setpoint.

Moving to Figure 5b, which reports the IMAP over a portion of the WHTC, the response of the model (teal line) differs significantly from the actual engine response (red line). It is important to remark that the simulation has been performed by providing the same boost pressure setpoint target requested by the real ECU during the experimental tests, which is represented by the grey line in Figure 5b. The differences between modelled and actual engine responses are not only in the values but also in their shapes. The actual engine achieved significantly lower IMAP values than those requested by the target due to the slow dynamics of the turbocharger and intake system. Instead, the preliminary simulation performed with the baseline engine model (teal line) shows a faster response and intake manifold pressure values which are closer to the desired one.

These results suggested the need for a detailed investigation on the reason of the mismatch between the predicted and experimental trends, in order to understand whether it was mainly due to a different response of the modelled controllers with respect to the real one, or to a non-accurate response of the engine sub models, including the air path.

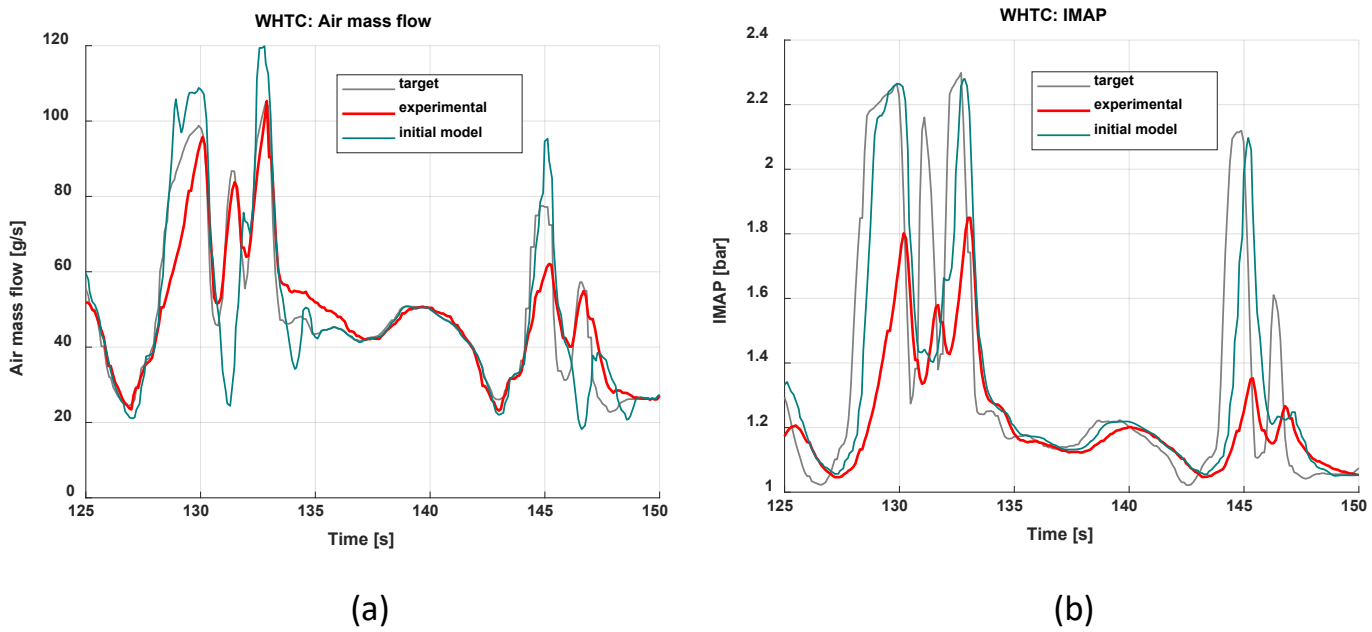
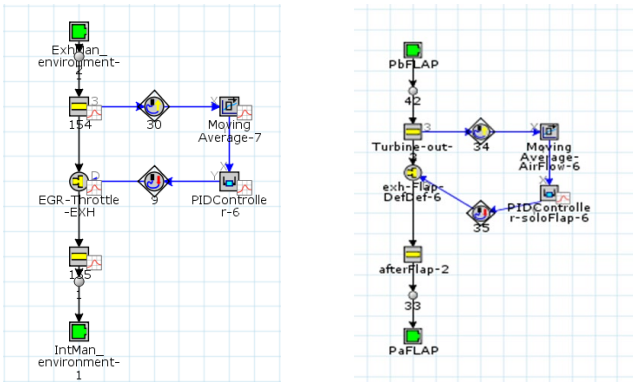


Figure 5. Transient performance of the initial baseline engine model over a portion of the WHTC: air mass flow rate (a) and IMAP (b)

Identification of correlations for the EGR, VGT and exhaust flap actuators

The initial step to improve the model performance was to isolate the physical response of the model from the effect of the EGR and VGT controllers. Therefore, these latter were removed from the model, and the experimental actuation signals measured in the real engine were set as inputs. In order to do so, correlations between the actuation variables used for the EGR valve, VGT rack and exhaust flap in the engine model, and the related experimentally acquired ECU signals (expressed in opening percentage) were built. This was needed as the ECU sends a command signal that ranges from 0 to 100% for the three actuators, while in the engine model the EGR valve and exhaust flap are commanded by setting an orifice diameter, while the VGT is actuated by setting the rack position, which ranges from 0 to 1. To build correlations for the EGR valve and exhaust flap, two virtual fluxing test benches were built as shown in Figure 6.



a) b)

Figure 6.Virtual flux benches to derive the correlations: a) EGR; b) Exhaust FLAP

Concerning the virtual flux bench to derive the EGR valve correlation, it can be seen than the inlet and outlet environments have been set at the pressure values measured during the actual experiments and a PID controller was free to modify the orifice diameter to obtain the EGR flow rate measured at the test-bed. Then, the opening signals from ECU and the valve diameters obtained from the virtual test bench were collected for each simulated engine point, and a correlation was built. Likewise, the exhaust flap valve correlation was obtained with the same procedure, by isolating the exhaust line right after the turbine until the aftertreatment, as shown in Figure 6b. In this case the virtual test bench was composed by an inlet environment, in which the experimental pressure downstream of the turbine was imposed, the flap valve, and an outlet environment, in which the experimental measured pressure downstream the flap was imposed. Again, a PID controller was free to change the flap valve diameter to match the experimental exhaust flow rate. The entire engine model was instead employed to build the VGT rack correlation. In particular, the previously built EGR and flap correlations were implemented in the model to manage these two actuations, and steady-state tests were simulated by setting the real ECU signals as inputs for the EGR valve and exhaust flap. The rack positions actuated by the VGT controller of the engine model were recorded and correlated to the real opening positions of the VGT actuator.

Figure 7 shows the obtained correlations for the EGR valve (Fig. 7a), exhaust flap (Fig. 7b) and VGT rack (Fig. 7c). The black points represent the raw data, while the red crosses represent the final correlation curve, obtained through polynomial fitting.

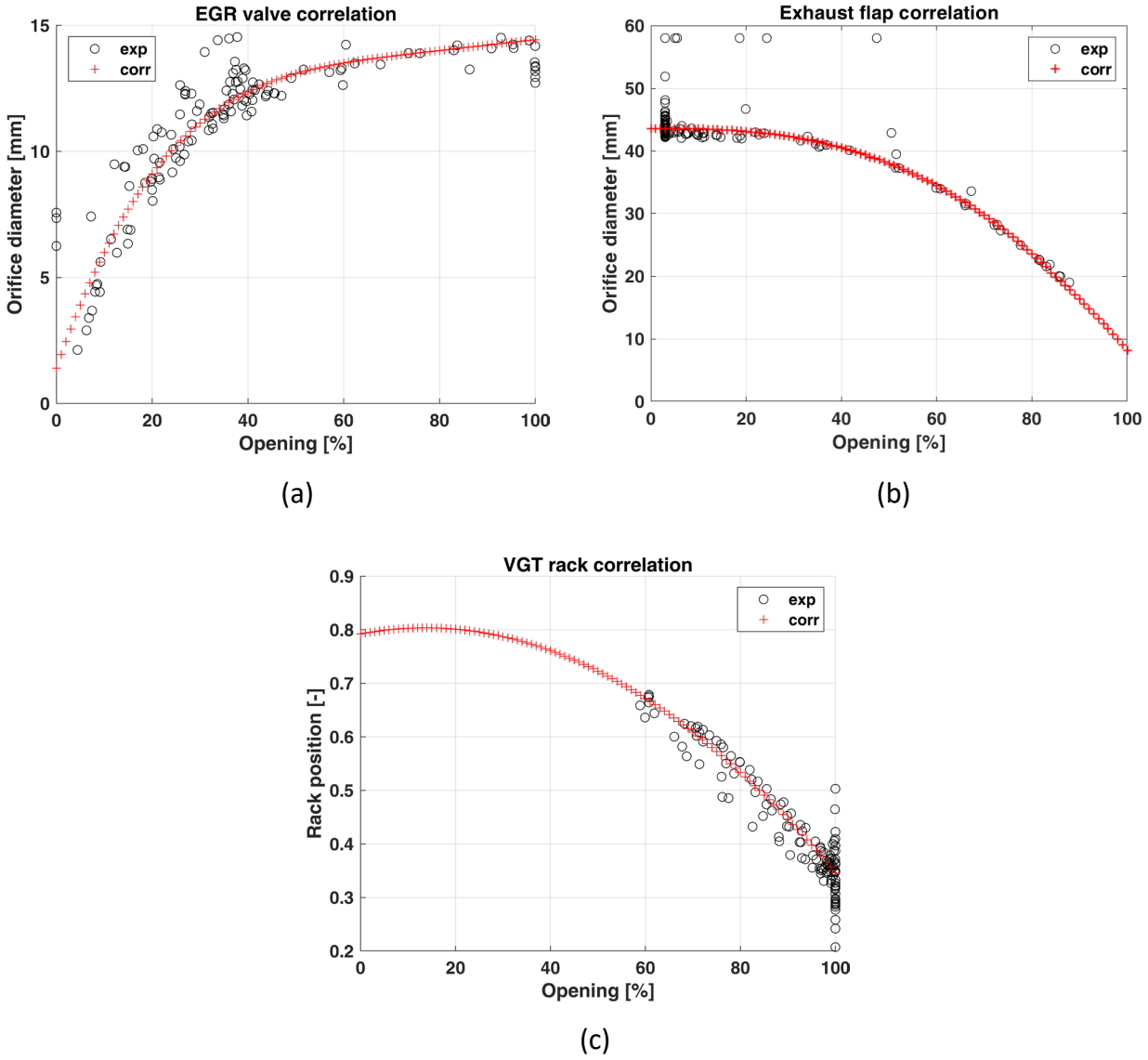


Figure 7. EGR valve correlation (a), FLAP valve correlation (b), VGT rack correlation (c)

It can be seen from the results of Fig. 7 that the correlations are satisfactory for all controllers. It can be seen, however, that a few outliers are present in the correlations. It was verified that in these points the pressure drop across the valve is very small, and as a consequence the influence of the valve diameter on the flow rate is low. This means that small uncertainties in experimental data or small inaccuracies in the model bring the controller to vary the valve diameter to a great extent, without matching the desired flow rate.

The VGT correlation is mostly linear and that experimental points do not show lower values than 60% of opening.

Transient simulations with experimental actuation profiles for EGR, VGT and flap

The previously developed correlations were then embedded in the engine model, and steady-state and transient simulations were repeated, by imposing the experimental actuator percentage positions coming directly from the ECU signals collected at the test bench. This approach will be indicated by the notation “ECU act” in the following charts.

The results for the most relevant variables at steady-state conditions are reported in Table 3. The results show that the model accuracy remains close to that of the initial model with baseline embedded controllers (see table 2).

Table 3. Validation, at steady-state conditions, of the model in which the experimental ECU actuation signals were imposed as inputs for the EGR/VGT/flap – The R2 and RMSE values were obtained by comparing the simulated and experimental results.

	R2	RMSE
BMEP	0.999	0.186 bar
Torque	0. 999	4.45 Nm

IMEP360	0.999	0.23 bar
EMAP	0.987	0.058 bar
IMAP	0.99	0.045 bar
Lambda	0.987	0.132
Xr	0.986	1.529 % (abs)
PFP	0.991	2.652 bar
Air	0.993	3.228 g/s
EGR	0.969	1.056 g/s
O2	0.935	0.262 % (abs)
NOx	0.847	91.719 ppm

After the steady-state validation, a WHTC was simulated to evaluate the performance of the model. The results in terms of air mass flow rate and IMEP are shown in Figures 8. The presence of two modelled curves which are indicated with "short pipe" and "long pipe" notations will be explained in the following paragraphs. For the moment, we focus on the results indicated as "short pipe" (black lines), which reflect the original geometry of the baseline model. From this simulation it emerged that, despite an improvement in the replication of boost pressure and air mass flow rate with respect to the baseline model, several differences with respect to the experimental values are still present, as it is possible to note by looking at the black lines in Figure 8a and 8b (ECU act, short pipe).

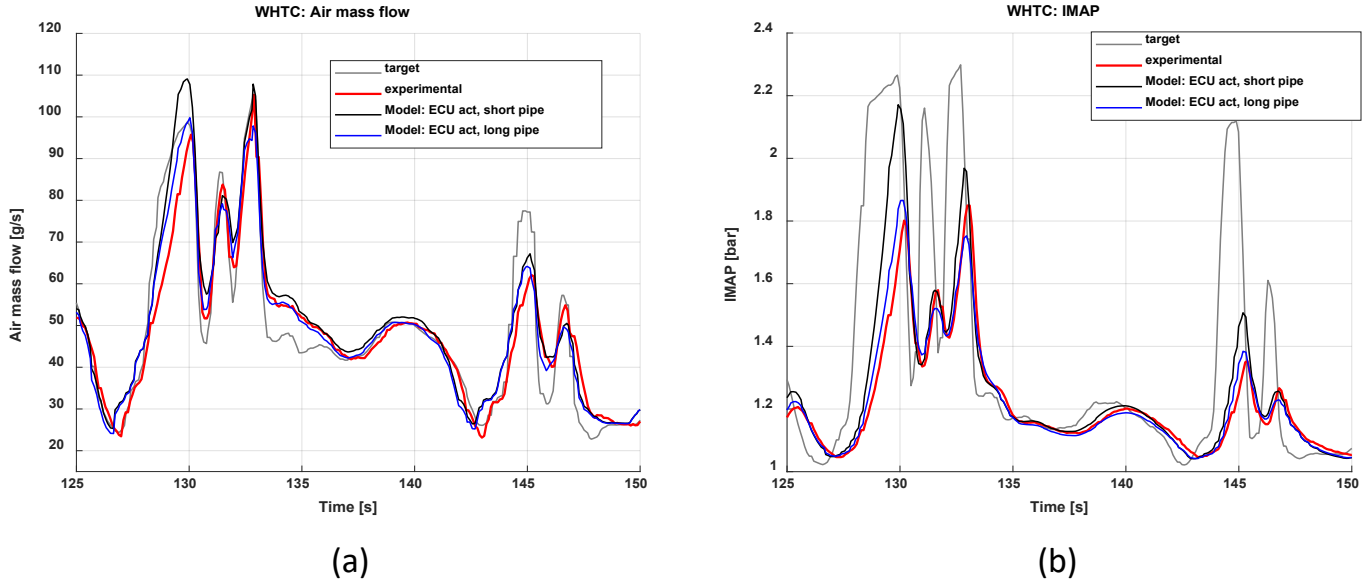


Figure 8. Transient performance of the model in which the experimental ECU actuation signals were imposed as inputs for the EGR/VGT/flap, over a portion of the WHTC: air mass flow rate (a) and IMAP (b). Two intake layouts were considered, i.e., that of the test bench ('long pipe'), and that of the stand-alone engine ('short pipe).

The authors started investigating this problem by focusing on the performance of the turbocharger group, including the moment of inertia and the characteristic maps of the compressor and turbine, and on the heat transfer in the exhaust manifolds. However, despite several simulations were carried out by modifying the tuning parameters of the turbine and compressor, as well as the heat transfer coefficients, the matching with the experimental results did not improve.

Therefore, the analysis focused on the air path geometry. A discrepancy between the model and the test bench experimental setup was identified in the air path circuit.

In particular, the original model (whose results are denoted as "short pipe" in Figure 8) featured an intake air path circuit that was representative of the stand-alone engine installed on the vehicle, but not of the engine installed at the test bed. In fact, a dedicated cooling circuit with an external cooler was realized at the test bench, in order to control the temperature of the engine coolant and of the air outflowing form the compressor, due to the lack of the frontal air on the radiator. Thus, additional pipes were installed to connect the engine to the external cooler, with a consequent increase in the overall length of the air path circuit with respect to that of the baseline engine. In order to account for this effect in the model, first the authors measured the volume of the additional pipes and of the external cooler. The volume of the pipes was calculated by measuring their diameter and length, while the internal volume of the external cooler was more difficult to evaluate, and therefore this estimation was affected by a high degree of uncertainty. To account for this uncertainty, the authors carried out several simulations by changing the length of the pipes upstream and downstream from the intercooler, in order to identify the configuration that better matched the transient behavior observed in the experimental tests. To do this, a Design of Experiment (DoE) was carried out, in which the additional pipe length was varied in a range between 3.5 m and 6.5 m, and the optimal configuration

was obtained for a pipe length of the order of 4.5 m. The model with this configuration is therefore referred to as “long pipe”, and is more representative of the test cell layout. .

The results obtained with the corrected intake geometry and imposing the experimental actuator position coming from the ECU signals, are reported in Figure 8a and 8b with blue lines (ECU act, long pipe). As it is possible to see, a major improvement has been obtained. The previous results are significant, since they show that the layout of the engine installed at the test bench can affect the transient behaviour to a great extent. Therefore, researchers should take these effects into account when designing the layout of the test bench, otherwise the transient performance of the tested engine could be not representative of the performance of the engine installed on the vehicle, especially when the research activity is focused on the analysis and/or control of the engine transient behaviour.

The model of the engine with the improved intake layout (“long pipe” with experimental actuators) was then tested also at steady-state operation. the complete validation results at steady state conditions are reported in Appendix A for the variables of major interest. It should be noted that the pipe length can also affect the engine performance at steady-state conditions, since it is directly correlated to the friction losses. However, the authors verified that this effect is not high, and therefore the related results were not reported in this paper for the sake of brevity.

Replication of the behaviour of the actual EGR and VGT controllers embedded in the engine ECU

After resolving the major issues related to the physics of the engine model, the focus shifted to the design of EGR and VGT controllers which are able to replicate the behaviour of the real ones implemented in the ECU. This was done with the objective to obtain the same experimental actuators command when providing the same experimental target to the modelled controllers. To this aim, two dedicated control systems were designed, the first one to govern the EGR valve and the second one to manage the VGT rack position.

The EGR control system was designed to control the air mass flow rate through the manipulation of the EGR valve in accordance with the regulation logic implemented in the ECU. The layout resembles the one of the ECU controller with a closed-loop PI regulator plus feedforward actions of EGR reference position and injected fuel quantity derivative.

Instead, the VGT rack regulation logic, which targeted the IMAP, consists of a PID with feedforward action based on the derivative of injected fuel mass and rack reference position.

The controllers were developed in Matlab Simulink, and the related schemes are reported in Appendix B.

Both controllers were provided with the same experimental targets as those of the real controllers, through the same maps, which are functions of engine speed and target load and are embedded in the ECU), in order to have consistent inputs. Furthermore their design has been performed independently by trying to obtain an actuator response which is as close as possible to the experimental one, since the two controllers are independent form each other. Subsequently, only a minor assessment was required when implementing both controllers at the same time. Their performance has been assessed with the use of the transient profiles introduced in the *Test description* section.

Figure 9 reports a comparison between the actuation commands of the modelled controllers (‘modeled’) and of the real ones (‘experimental’), concerning the EGR controller (Fig. 9a) and the VGT controller (Fig. 9b), over a portion of the WHTC. It is possible to see how the EGR valve experimental profile (red line) is well reproduced by the designed EGR controller (black line). Only minor differences can be observed over which the experimental controller shows a more aggressive behaviour in both closing direction (time t = 890 s) and opening direction (time t = 870 s and time t = 930 s). Still, these differences can be tolerated, as they are in line with the engine model accuracy in reproducing the physical behaviour of the system.

As far as the VGT controller is concerned (Fig. 9b), it is possible to see that the behaviour of the designed control system (black line) reproduces that of the real controller (red line) with a good level of accuracy, even though some differences occur over the considered WHTC interval. The main deviations are due to the threshold of activation and rates of closing and opening of the rack position. The designed controller is, in general, less aggressive in both opening and closing directions. However, the result was considered acceptable, since it was verified that the actuation produced by the modeled VGT controller allows to obtain a response, in terms of IMAP, which is very close to the experimental one for the considered transient tests, as it will be shown in the *Transient validation* section.

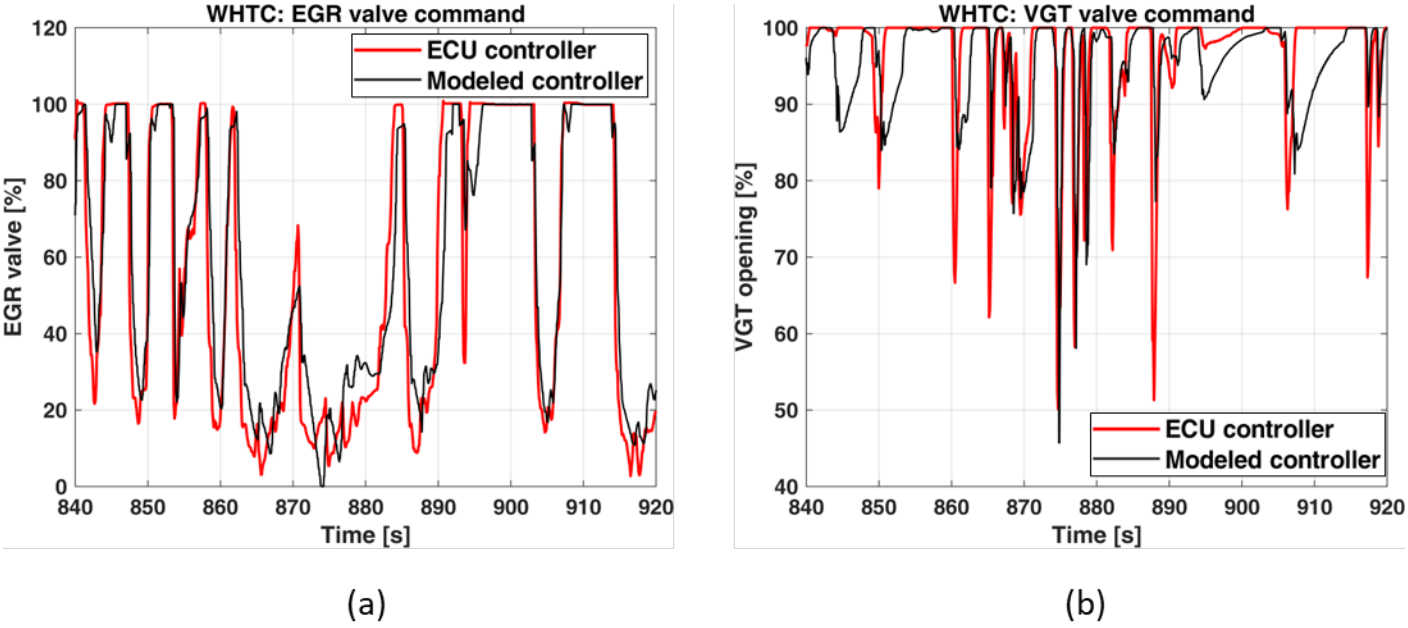


Figure 9. Comparison between the actuation commands of the modelled controllers ('modeled') and of the real ones ('experimental'), over a portion of the WHTC: a) EGR; b) VGT

After the assessment, the EGR and VGT controllers were embedded in the engine model, and a simulation of the WHTC was repeated, with the two intake layouts considered in the previous section (refer to Fig. 8), which are referred to as "short pipe" and "long pipe"). Figure 10 shows the results, in terms of air mass flow (Fig. 10a) and IMAP (Fig. 10b) over a portion of the WHTC .

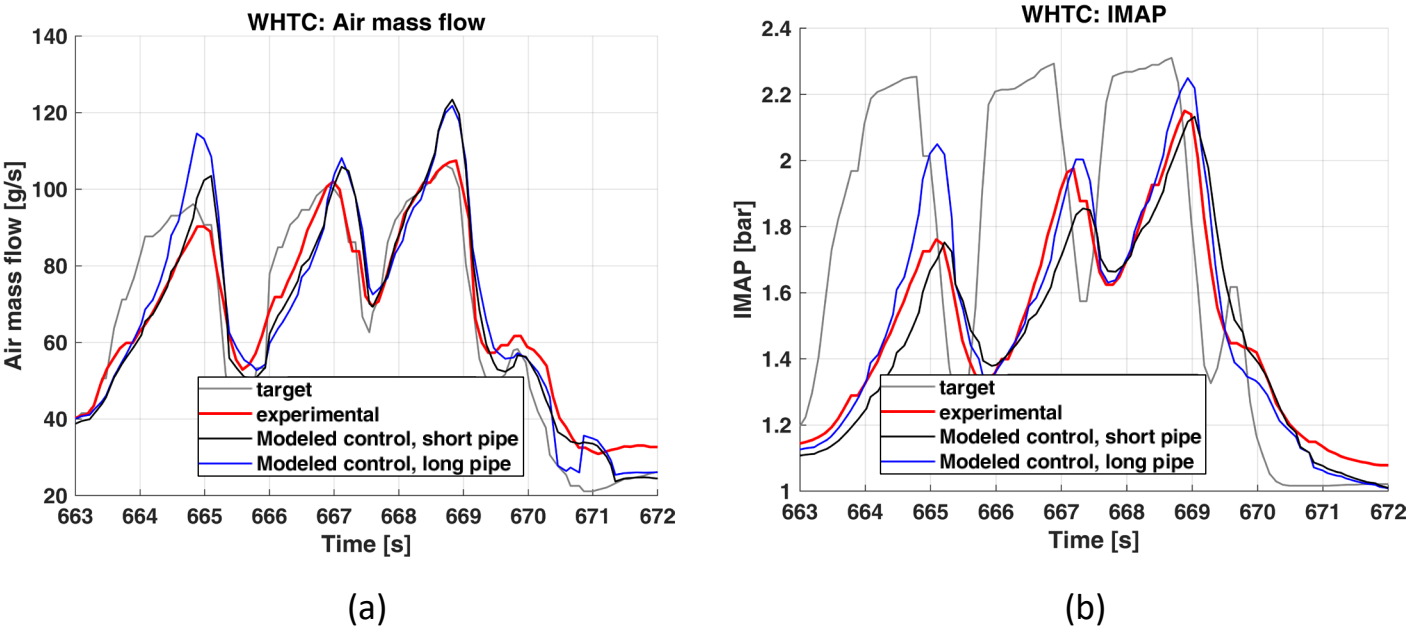


Figure 10. Transient performance of the final model which includes the developed air-path controllers, over a portion of the WHTC: air mass flow rate (a) and IMAP (b). Two intake layouts were considered, i.e., that of the test bench ('long pipe'), and that of the stand-alone engine ('short pipe).

From Figure 10a it is possible to see that the air mass flow rate expresses a faster response with a greater slope than the experimental result when the shorter layout is used (blue line), while the model that implements the test cell layout (black lines) reproduces the experimental profile more accurately. This is particularly evident at time t = 664s.

The influence of the layout is even more significant when looking at the IMAP trend, which is shown in Figure 10b. Here the difference in slope between the blue line, that corresponds to the short pipe configuration, and the red line, which is representative of the experimental layout, is particularly

evident especially around t= 665s. On the contrary, the black line, that corresponds to the longer volume shows a response which is overall more similar to the experimental one (red line).

To conclude the analysis, Figures 11a and 11b show, for the same time interval, the commands of the EGR and the VGT valves, respectively. It can be seen that the EGR valve and VGT actuations are slightly affected by the engine layout This reflects the faster dynamics of the short circuit with respect to the longer one.

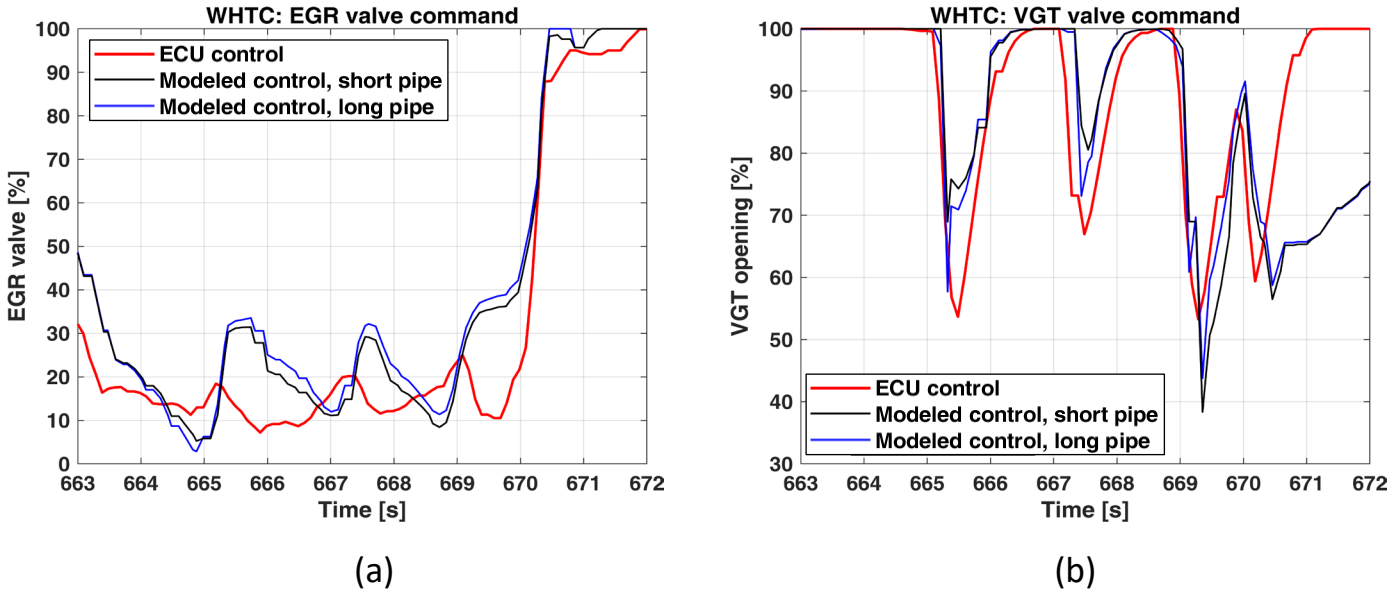


Figure 11. Transient performance of the final model which includes the developed air-path controllers, over a portion of the WHTC: EGR valve actuation (a) and VGT actuation (b). Two intake layouts were considered, i.e., that of the test bench ('long pipe'), and that of the stand-alone engine ('short pipe).

Transient validation

This section presents the validation of the developed model with embedded air-path controllers and long pipe configuration (denoted as 'final model'), in transient conditions, by comparing the predicted values of several engine variables with respect to the experimental ones. The model included the layout of the test bench, which corresponds to the long inlet pipe configuration. Figures 12-14 show the main results for the speed/load ramp (Fig. 12), and for the WHTC over two different time intervals (Figure 13, 14). In the figures, the targets are indicated in gray, the experimental data in red, the initial baseline model results (with standard controllers) in teal and the final model results with the air-path controllers in black.

The first test is a section of the speed/load ramp, (refer to the *Test description* Section). Figures 12a and 12b report the results for the air mass flow and IMAP, respectively.

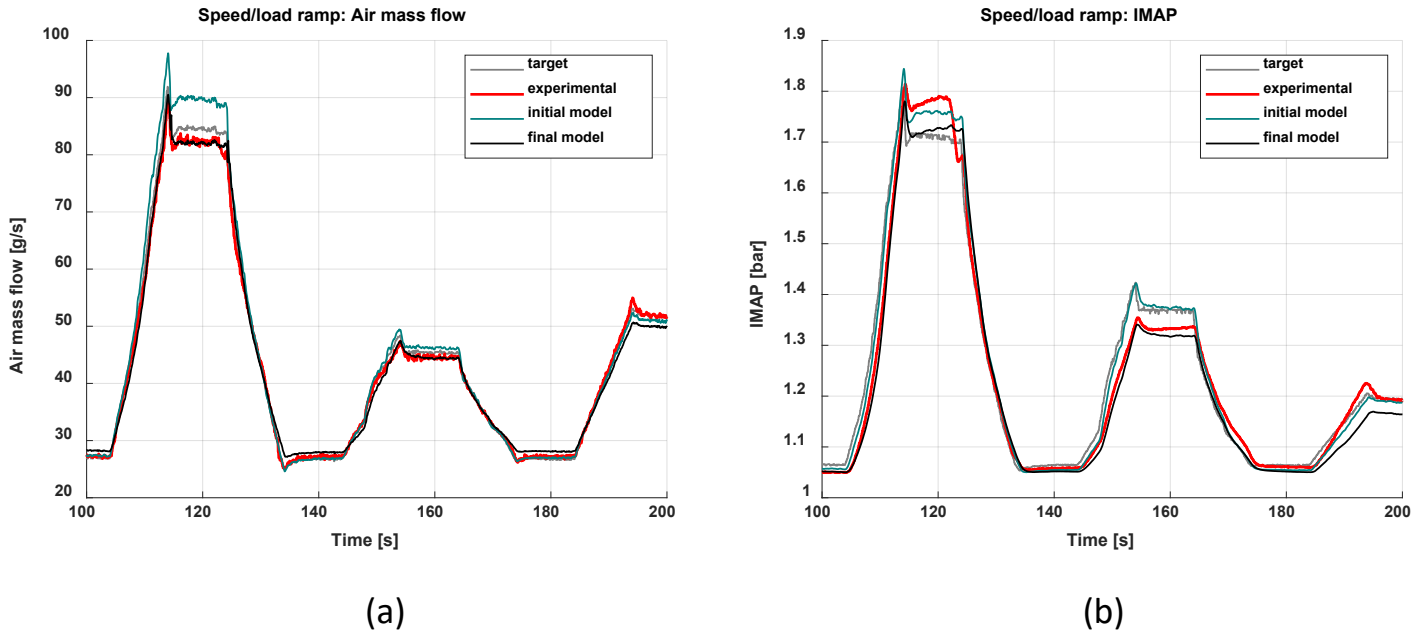


Figure 12. Transient performance of the initial and final engine models, over a portion of the speed/load: Air mass flow rate (a) and IMAP (b).

Figure 12a shows that with the introduction of the final model, which includes the assessed air-path controllers (black line) replicates the experimental result (red line) correctly. It is important to remark that the simulation has not been performed using as target the experimental value of the air mass flow, but both cases ('final model' and 'experimental') share the same target which is obtained from the look-up table embedded in the ECU. Instead, in the initial model EGR fraction target was used instead of the air mass flow rate (i.e., the quantity that is used in the real engine controller). In this case, around time t = 120s, an excess of air supply is obtained.

Figure 12b reports the IMAP result. Here it is possible to see how the final model achieves a slightly worse response than the experimental actuation (red line) at the beginning and at the end of the considered interval. This is mainly caused by the conservative approach chosen during the design process of the VGT control system. Nonetheless, the overall performance of the final model remains close to the experimental one. The initial model instead showed a more aggressive response producing a faster engine response than the experimental one.

The most interesting results can be seen by looking at the WHTC cycle (Figs 13, 15), since it shows a higher transient content in terms of engine speed and load. Figure 13, 15 reports the transient performance of the initial and final engine models over the WHTC for 4 different time intervals: t=125-150s (Figs. 13a, c, e), t=645-675s (Figs. 13b, d, f), t=840-920s (Figs. 15b, d, f) and t=1620-1760s (Figs. 15b, d, f). The values of BMEP (a, b), IMAP (c, d) and air mass flow (e, f) are reported. Figure 14 reports instead the injected fuel quantity, for the time interval t=125-150s.

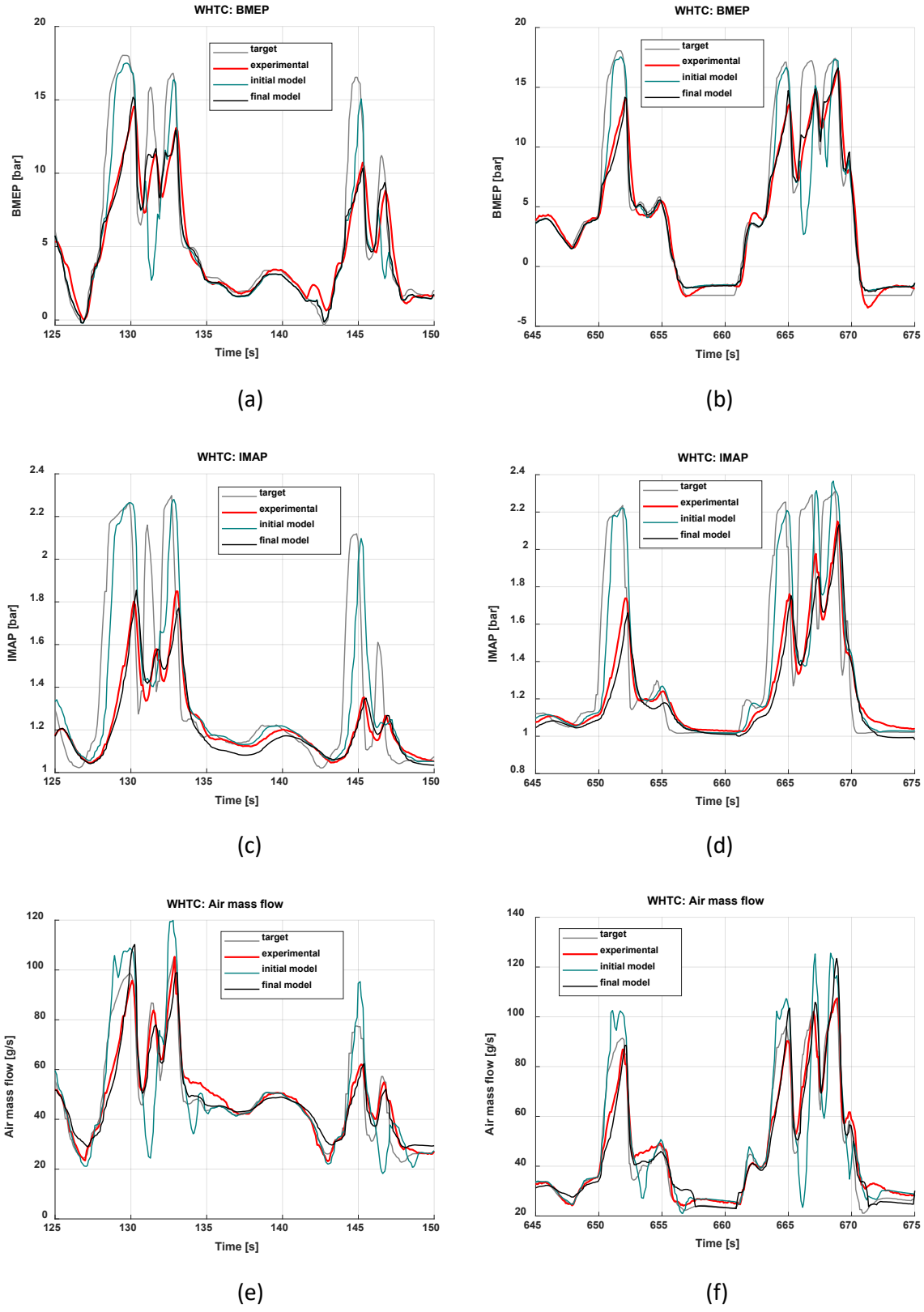


Figure 13. Transient performance of the initial and final engine models over the WHTC for two different time intervals: t=125-150s (a, c, e), t=645-675s (b, d, f). The values of BMEP (a, b), IMAP (c, d) and air mass flow (e, f) are reported.

Figure 13a shows how the BMEP obtained experimentally is accurately reproduced over the considered time interval by the final model. Moreover, the introduction of the enhanced air-path control system in the model allows to reproduce the "smoke-limit" fuel cuts imposed by the ECU at time t = 130s and time t = 145 s. As it is possible to see, in fact, the behaviour of the initial baseline model significantly deviates from the experimental response achieving values which are close to the required BMEP target and significantly higher than the actual ones. In fact, during the experimental tests, the engine does not deliver the required BMEP due to a lack of air, which is caused by a delay in the boost pressure rise. This effect is well reproduced by the final engine model, while the initial one completely ignores this effect and leads to an engine response which is closer to the target but very different from the experimental one.

Figure 13e shows that the air mass flow rate of the final model is very close to the experimental result with only a significant overshoot at time t =130 s. Comparing the performance of the initial and final models it is noticeable that the first one achieved higher air mass flow rates than the latter one. Furthermore, its response is faster and affected by the presence of gaps at times t =132s and t =147 s. These instants correspond to the lack of BMEP observed in Figure 13a.

In Figure 13c it can be seen that also the IMAP obtained with the final model is very close to the experimental measurement. It is important to remark that both initial and final models exploited the same target seen by the actual engine at the test bench. The final model well reproduces the actual dynamics of the IMAP very accurately, showing a significant lag in the response and achieving lower value than the target requested during fast transients, as it occurs on the real engine. Instead, the initial model shows a response that is very different from that observed experimentally.

The second section of the WHTC which is reported in Figures 13b,d,f) ranges from time t = 645 s to time t =675 s. This section allows to emphasize the cut of fuel induced by the ECU due to the lack of air supply. In Figure 13b the effect of the fuel limitation is visible at time t = 650 s, t = 664 s and t = 669 s. As a consequence, the engine achieved a lower BMEP than the demanded one. The final model correctly reproduces the actual engine response, while the initial model leads to a quicker response than that of the real engine.

As it is shown in Figure 13f, the final model response in terms of air mass flow is significantly improved with respect to the initial one. The rising and falling slopes are correctly reproduced and the surplus of air supply is only limited to local overshoots time t = 665 s and t = 669s.

The IMAP results presented in Figure 13d are consistent with those previously presented over the previous section of the WHTC and the BMEP and air mass flow above commented. The final model correctly reproduces the behaviour of the real engine in both shape and values. It can also be noticed that the control introduces a small lag in the response. This is due to the conservative approach used in the definition of controller parameters. Instead, the initial model produced a response that differs significantly from the experimental one in both shape and values.

A focus on the combustion side is also reported concerning the time interval between t=125-150s. In particular, Figure 14 reports the injected fuel quantity as a function of time for the initial and final models, as well as the experimental trend. It is possible to see that the final model accurately reproduces the behaviour of the actual engine showing the same shape and values. Furthermore, the final model also shows the reproduction of the fuel limitation occurred over the actual engine due to the lack of air supply and constraint on smoke production. The initial model was not able to capture these limitations, moreover it showed relevant gaps while facing an increasing load request.

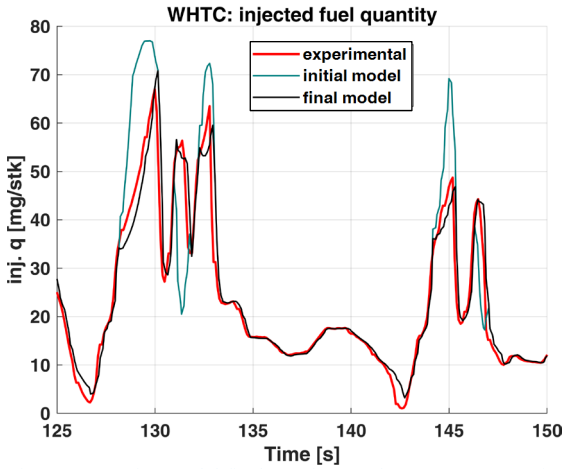


Figure 14. Engine model final transient performance. WHTC time t = 125 to 150s, injected fuel quantity

The third section of the WHTC presented in figure 15 (a, c ,e) ranges from time t = 840 s to time t =920 s. This section allows to see the performance of the final model over a longer time span than the previous figures and includes a variety of conditions from aggressive to smooth.

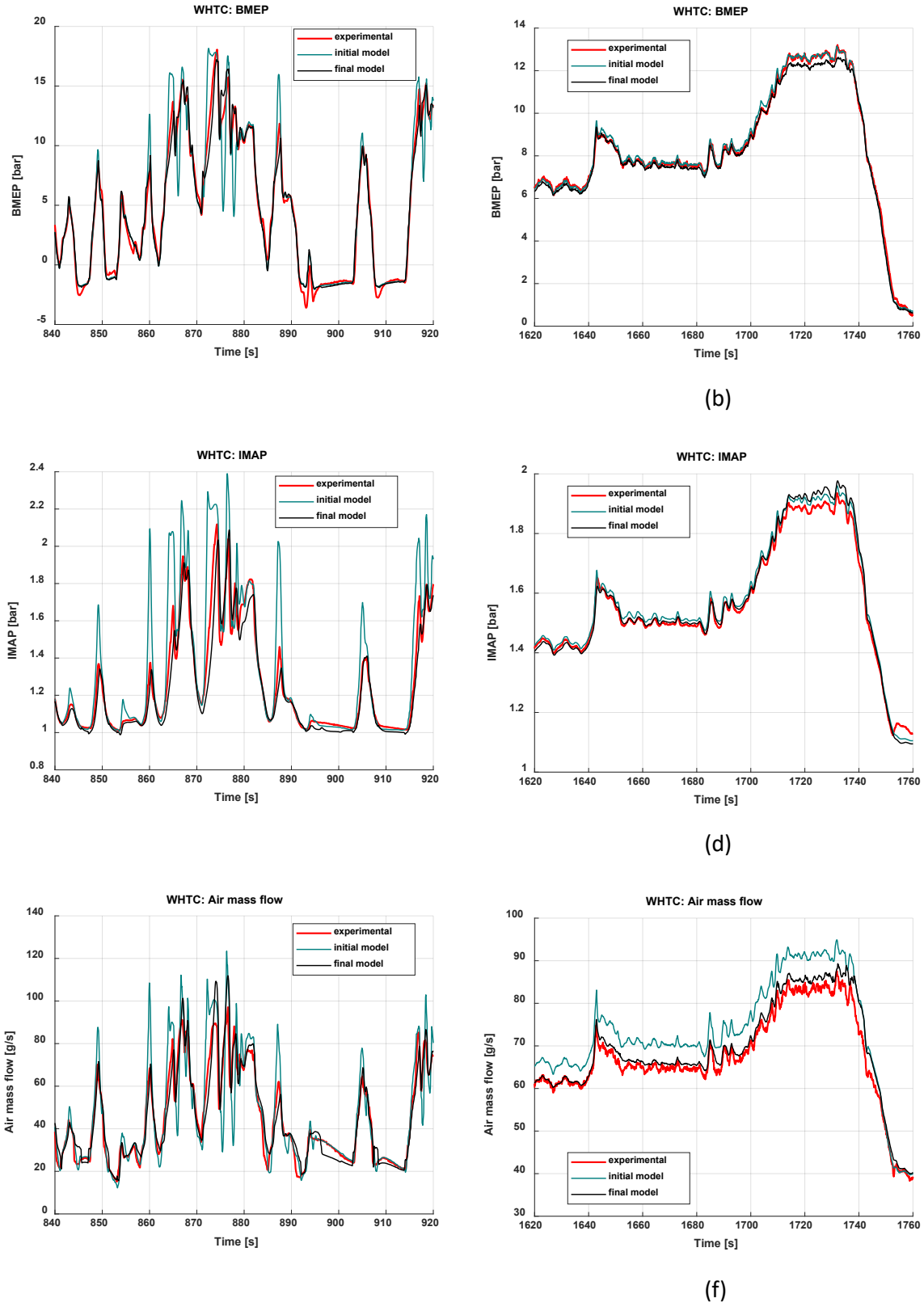


Figure 15. Transient performance of the initial and final engine models over the WHTC for two different time intervals: t=840-920s (a, c, e), t=1620-1760s (b, d, f). The values of BMEP (a, b), IMAP (c, d) and air mass flow (e, f) are reported.

It can be seen that the BMEP is well reproduced, avoiding both over- and under-shoots. Some deviations are present around time t=890 s when the BMEP is negative but they can be ascribed to the model itself and not the control systems, as both controllers and injection are off. On the other hand, the initial model presented multiple overshoots and load gaps over this considered time span.

Figure 15e reports the air mass flow. The final model shows only limited overshoots with respect to the experimental results between time t = 870 s and t = 880 s. Furthermore, the dynamics of the response is well reproduced.

The IMAP results presented in Figure 15c show that the final model correctly reproduces the response of the engine although being slightly less aggressive. Instead, the initial model produced a very sharp response that differs significantly from the experimental one.

Figures 15b, d, f report the results over the WHTC in a time range from t =1620 s to t = 1760 s. This section of the test is characterized by an almost stationary condition in between smooth transitions and therefore can be used to expose modeling error due to offsets and drifts. Figure 15b shows that the BMEP is well reproduced by the initial and final models, thus confirming that transient effects are more limited over this time interval.

Figure 15d shows that the IMAP is well reproduced by both the initial and the final model with minor deviations from time t = 1640 to time t = 1680 s for the initial and from time t = 1715 s to time t = 1740 for the final one.

Finally, table 4 reports the percentage differences of the simulated cumulative injected fuel, with respect to the experimental data, for the three considered engine models. The initial and the 'ECU act, long pipe' models show the largest deviations in the injected fuel. This is due to the fact that both models simulate higher air mass flow rates with respect to the actual engine, which lead to a higher amount of injected fuel. The first two models, as previously seen, are not able to capture the fuel cut phases which occur in the real engine, due to delayed boost pressure response, while the final model is able to reproduce this effect.

Table 4. Percentage deviation of cumulative injected fuel with respect to the experimental data.

	Deviation of cumulative injected fuel
Initial model	3.9 %
ECU act, long pipe	4.8 %
Final model	1.6 %

Final considerations and summary of the proposed approach

Figure 16 reports a scheme of the methodology that was presented in this paper to assess the model performance in transient operation. For the sake of clarity, the authors also reported, for the main steps, a reference to the relevant figures that were presented in the paper.

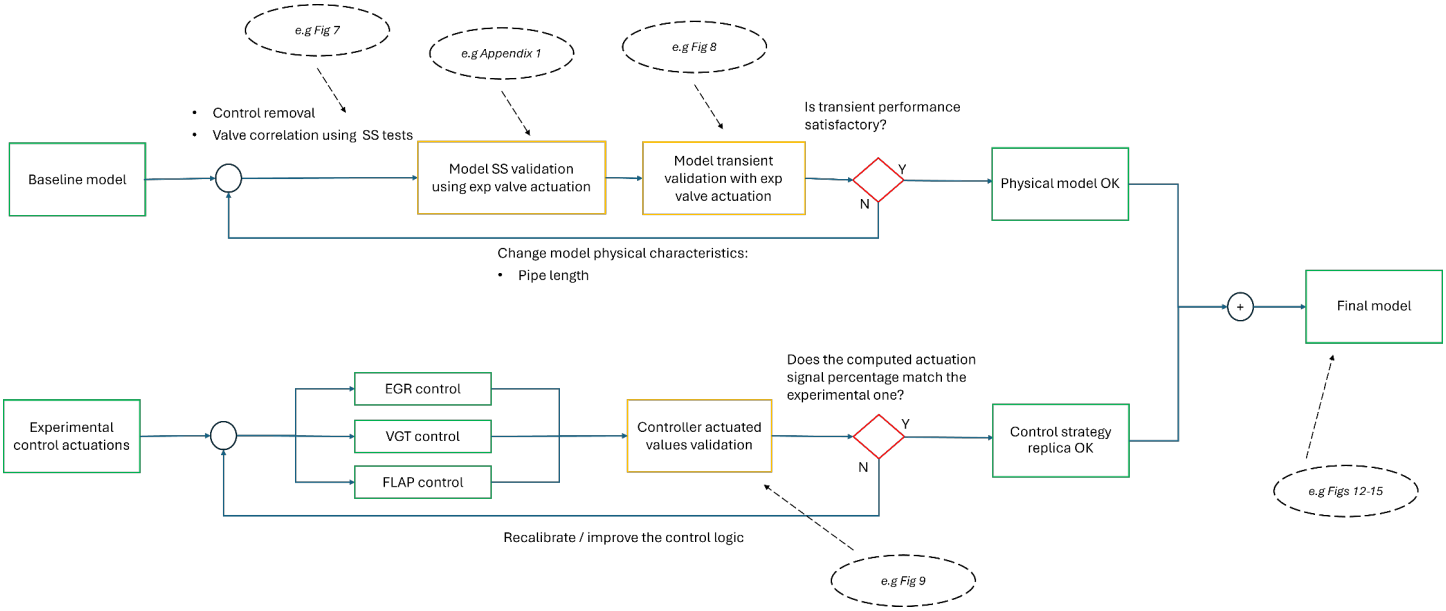


Figure 16 Flow chart of the methodology for the assessment of the model.

The first step consists of a verification of the consistency of the physical model. In this phase, all controllers are removed, and correlations are identified between the control variables of the actuators which are used in the model, and the control variables which are used in the real engine. This allows to set the control signals of the real engine as input for the model, in order to check its physical consistency and correct possible mistakes in the modelling, as it was done in this paper with the correction of the intake pipe length. However, possible inconsistencies may also be related to the turbocharger group performance and inertia, to the heat transfer or to other parameters.

The second step consists in the design of the controllers, in order to replicate the same behaviour which is observed in the real engine.

The two previous steps allow to obtain a complete engine model which is able to replicate the behaviour of the real engine in an accurate way, and which features the same control variables of the actuators (EGR, VGT, flap) and the same control logics.

It should also be noted that the physical model and the control logics of the actuators were assessed independently. Therefore, the engine model features a very accurate physical response, so that it can be used to develop and test also new controllers (different from the original ones). Vice versa, the original engine controller can be implemented in modified or different engine models in order to test its functionality. Moreover, the fact that the developed physical model and control logics give an accurate results when coupled together, confirm the consistency with respect to the real engine behaviour. Thus, the model can be used for several applications, including:

- The development and assessment of innovative control algorithms by means of the Model-in-the-Loop methodology.

- A detailed analysis and testing of the behaviour of the control logics of the real engine in different scenarios.

- The development of detailed dynamic vehicle models, in which the engine model is integrated so as to evaluate its performance in dynamic driving conditions.

Conclusions

A systematic methodology for assessing the transient performance of a 1-D model of a diesel engine for heavy-duty applications was presented in this study. The main objective was to reproduce the actual dynamic response of the real engine, including its air-path controllers, over several transient profiles. The starting point for the analysis was a previously developed baseline engine model, which featured an accurate behaviour at steady-state conditions, but not in transient operation. The transient model response was improved through several steps. First, the air-path controllers were removed, in order to analyse the physical response of the system when setting the experimental actuation signals as inputs for the EGR and VGT actuators. This allowed to identify a mismatch between the intake layout of the engine installed at the test bench and the modelled one, which was representative of the stand-alone commercial engine. It was verified that the impact of the test bench layout on the engine transient performance is not negligible, an aspect that is not widely discussed in the literature. Therefore, researchers should take these effects into account when designing the layout of the test bench, otherwise the transient performance of the tested engine could be not representative of the performance of the engine installed on the vehicle, especially when the research activity is focused on the analysis and/or control of the engine transient behaviour. The following steps included the assessment of the EGR and VGT controllers, in order to mimic the behaviour of the actual controllers embedded in the ECU, and their implementation in the model. The latter was finally tested over the WHTC and over a custom load/speed ramp, The obtained results show that the model is able to reproduce the engine response as well as the actuations over a WHTC in an accurate way, also including fuel cut-off phases due to delayed boost pressure response. Therefore, the proposed methodology is effective in obtaining a very accurate dynamic response of the engine model. The latter is suitable for several applications, including virtual calibration and Model-in-the-loop testing of innovative control algorithms.

References

1. Jalivar, G.; Saray, R.K.; Neshat, E. Investigation of PCCI Combustion and Emissions of Biodiesel Fuel at Low Load Conditions Using Design of Experiment (DOE). *J Therm Anal Calorim* **2023**, *148*, doi:10.1007/s10973-022-11864-w.
2. Ram, V.; Salkuti, S.R. An Overview of Major Synthetic Fuels. *Energies (Basel)* 2023, *16*.
3. Mancarella, A.; Marello, O. Effect of Coolant Temperature on Performance and Emissions of a Compression Ignition Engine Running on Conventional Diesel and Hydrotreated Vegetable Oil (HVO). *Energies (Basel)* **2023**, *16*, doi:10.3390/en16010144.
4. Djamari, D.W.; Idris, M.; Paristiawan, P.A.; Abbas, M.M.; Samuel, O.D.; Soudagar, M.E.M.; Herawan, S.G.; Chandran, D.; Yusuf, A.A.; Panchal, H.; et al. Diesel Spray: Development of Spray in Diesel Engine. *Sustainability (Switzerland)* 2022, *14*.
5. Ferrari, A.; Novara, C.; Vento, O.; Violante, M.; Zhang, T. A Novel Fuel Injected Mass Feedback-Control for Single and Multiple Injections in Direct Injection Systems for CI Engines. *Fuel* **2023**, *334*, doi:10.1016/j.fuel.2022.126670.
6. D'Ambrosio, S.; Ferrari, A.; Mancarella, A.; Mancò, S.; Mittica, A. Comparison of the Emissions, Noise, and Fuel Consumption Comparison of Direct and Indirect Piezoelectric and Solenoid Injectors in a Low-Compression-Ratio Diesel Engine. *Energies (Basel)* **2019**, *12*, doi:10.3390/en12214023.
7. Ventura, L.; Malan, S.A. Air Path and Combustion Controls Coordination in Diesel Engine. In Proceedings of the International Conference on Control, Automation and Systems; 2022; Vol. 2022-November.
8. Malan, S.A.; Ventura, L.; Manelli, A. Cycle to Cycle Closed-Loop Combustion Control through Virtual Sensor in a Diesel Engine. In Proceedings of the 2021 29th Mediterranean Conference on Control and Automation, MED 2021; 2021.
9. d'Ambrosio, S.; Finesso, R.; Hardy, G.; Manelli, A.; Mancarella, A.; Marello, O.; Mittica, A. Model-Based Control of Torque and Nitrogen Oxide Emissions in a Euro VI 3.0 L Diesel Engine through Rapid Prototyping. *Energies (Basel)* **2021**, *14*, doi:10.3390/en14041107.

10. Cococcetta, F.; Finesso, R.; Hardy, G.; Marello, O.; Spessa, E. Implementation and Assessment of a Model-Based Controller of Torque and Nitrogen Oxide Emissions in an 11 L Heavy-Duty Diesel Engine. *Energies (Basel)* **2019**, *12*, doi:10.3390/en12244704.

11. Ou, S.; Yu, Y.; Yang, J. Study on the Closed-Loop Combustion Control for a Diesel Engine by Using a Dynamic-Target Online Prediction Model. *Control Eng Pract* **2022**, *125*, doi:10.1016/j.conengprac.2022.105226.

12. Ventura, L.; Finesso, R.; Malan, S.A. Development of a Model-Based Coordinated Air-Fuel Controller for a 3.0 Dm3 Diesel Engine and Its Assessment through Model-in-the-Loop. *Energies (Basel)* **2023**, *16*, doi:10.3390/en16020907.

13. Jacob, A.; Ashok, B. An Interdisciplinary Review on Calibration Strategies of Engine Management System for Diverse Alternative Fuels in IC Engine Applications. *Fuel* **2020**, *278*, doi:10.1016/j.fuel.2020.118236.

14. Özgül, E.; Şimşek, M.; Bedir, H. Use of Thermodynamical Models with Predictive Combustion and Emission Capability in Virtual Calibration of Heavy Duty Engines. *Fuel* **2020**, *264*, doi:10.1016/j.fuel.2019.116744.

15. Bolu, S.; Ozgul, E.; Epguzel, E.; Gurel, C. Use of Thermodynamic Models for Compression Ratio and Peak Firing Pressure Optimization in Heavy-Duty Diesel Engine. *Energy* **2022**, *248*, doi:10.1016/j.energy.2022.123311.

16. Ermakov, A.; Salakhov, R.; Khismatullin, R. Application of Numerical Simulation Methods to Improve the Efficiency of Cooling Systems. In Proceedings of the Proceedings of the 2023 5th International Youth Conference on Radio Electronics, Electrical and Power Engineering, REEPE 2023; 2023.

17. Wang, Q.; Yao, H.; Yu, Y.; Yang, J.; He, Y. Establishment of a Real-Time Simulation of a Marine High-Pressure Common Rail System. *Energies (Basel)* **2021**, *14*, doi:10.3390/en14175481.

18. Jin, Z.; Vento, O.; Zhang, T.; Ferrari, A.; Mittica, A.; Ouyang, L.; Tan, S. Numerical-Experimental Optimization of the Common-Feeding Injection System Concept for Application to Light-Duty Commercial Vehicles. *Journal of Energy Resources Technology, Transactions of the ASME* **2021**, *143*, doi:10.1115/1.4050133.

19. Gowrishankar, S.; Krishnasamy, A. Parametric Optimization with Biodiesel-Water Emulsion under Premixed Lean Combustion to Achieve High Efficiency and Clean Combustion. *Fuel* **2023**, *344*, doi:10.1016/j.fuel.2023.128098.

20. Pla, B.; De La Morena, J.; Bares, P.; Jiménez, I. Adaptive In-Cylinder Pressure Model for Spark Ignition Engine Control. *Fuel* **2021**, *299*, doi:10.1016/j.fuel.2021.120870.

21. D'Ambrosio, S.; Iemmolo, D.; Mancarella, A.; Salamone, N.; Vitolo, R.; Hardy, G. Zero Dimensional Models for EGR Mass-Rate and EGR Unbalance Estimation in Diesel Engines. In Proceedings of the SAE Technical Papers; 2017; Vol. 2017-September.

22. Samuel, J.; Ramesh, A. An Improved Physics-Based Combustion Modeling Approach for Control of Direct Injection Diesel Engines. *SAE Int J Engines* **2020**, *13*, doi:10.4271/03-13-04-0030.

23. Ljung, L. Black-Box Models from Input-Output Measurements. In Proceedings of the Conference Record - IEEE Instrumentation and Measurement Technology Conference; 2001; Vol. 1.

24. Can, Ö.; Baklacioglu, T.; Özturk, E.; Turan, O. Artificial Neural Networks Modeling of Combustion Parameters for a Diesel Engine Fueled with Biodiesel Fuel. *Energy* **2022**, *247*, doi:10.1016/j.energy.2022.123473.

25. Ventura, L.; Malan, S.A. Recurrent Neural Network to Estimate Intake Manifold O2concentration in a Diesel Engine. In Proceedings of the International Conference on Control, Automation and Systems; 2020; Vol. 2020-October.

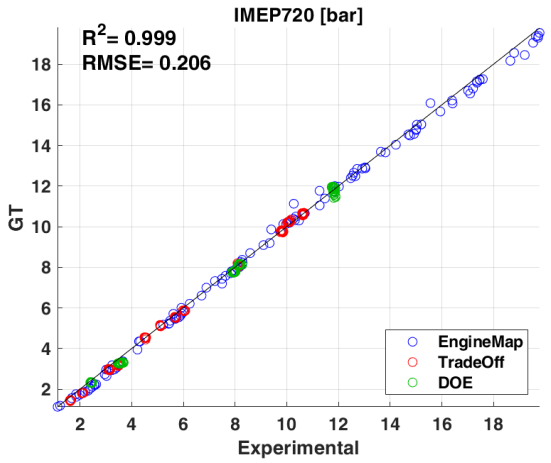
26. Steinhauser, M.O. *Computer Simulation in Physics and Engineering*; 2012;

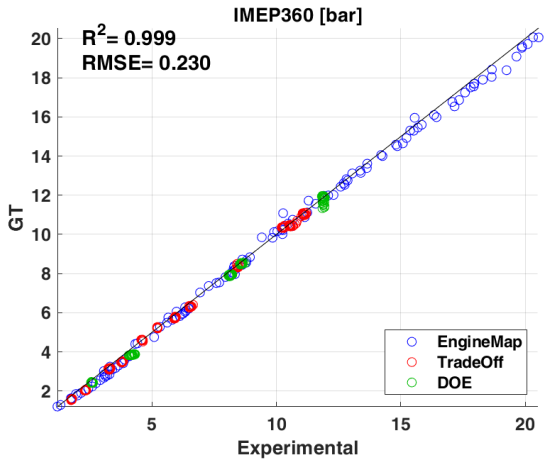
Definitions/Abbreviations

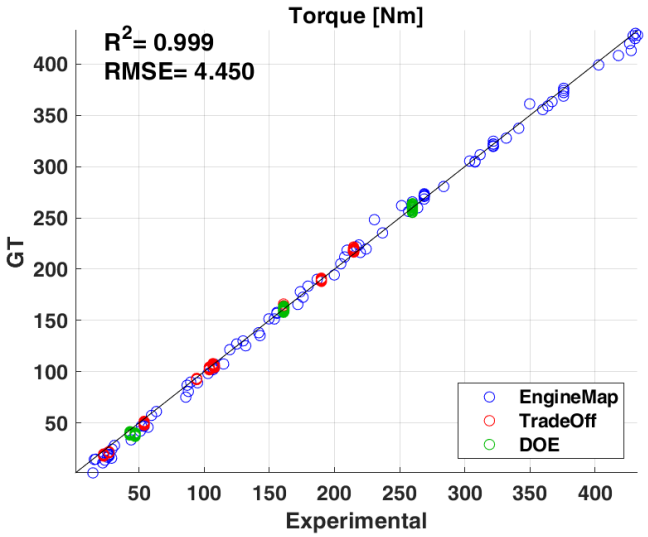
BMEP	Brake Mean Effective Pressure
DOE	Design of Experiment
ECU	Electronic Control Unit
EGR	Exhaust Gas Recirculation
ICE	Internal Combustion Engine
IMAP	Intake Manifold Pressure
NO_x	Nitrogen Oxides

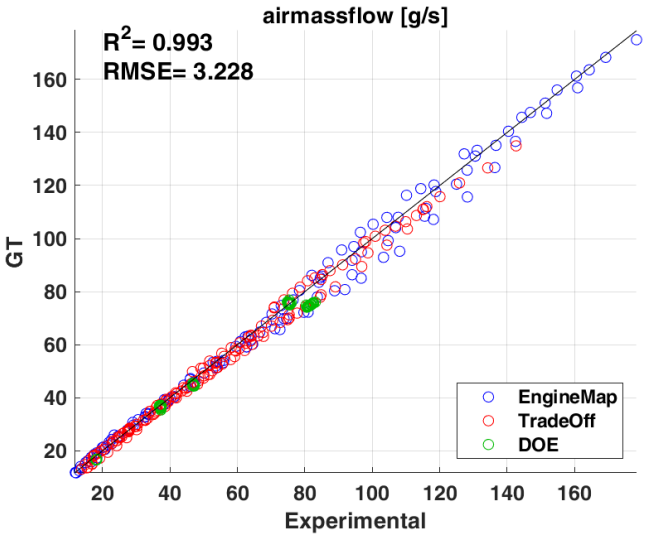
RMSE	Root Mean Square Error
RPM	Revolution per Minute
SS	Steady-State
VGT	Variable Geometry Turbine
WHTC	World- Harmonized Transient Cycle

Appendix A









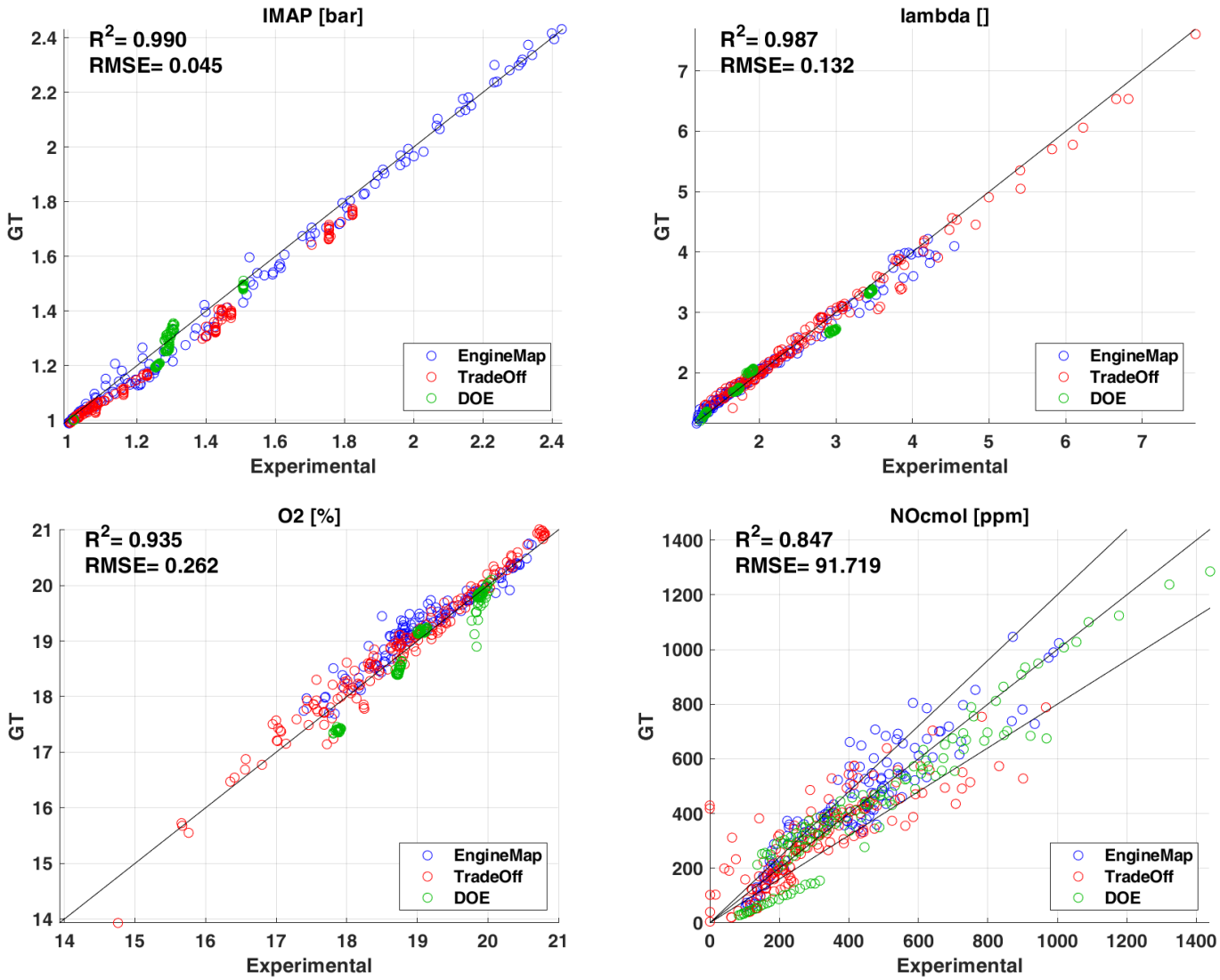


Figure A1. Validation of the engine model, in which the experimental ECU actuation signals are set as inputs for the EGR, VGT and exhaust flap, at steady-state conditions

Appendix B

EGR Open loop branch

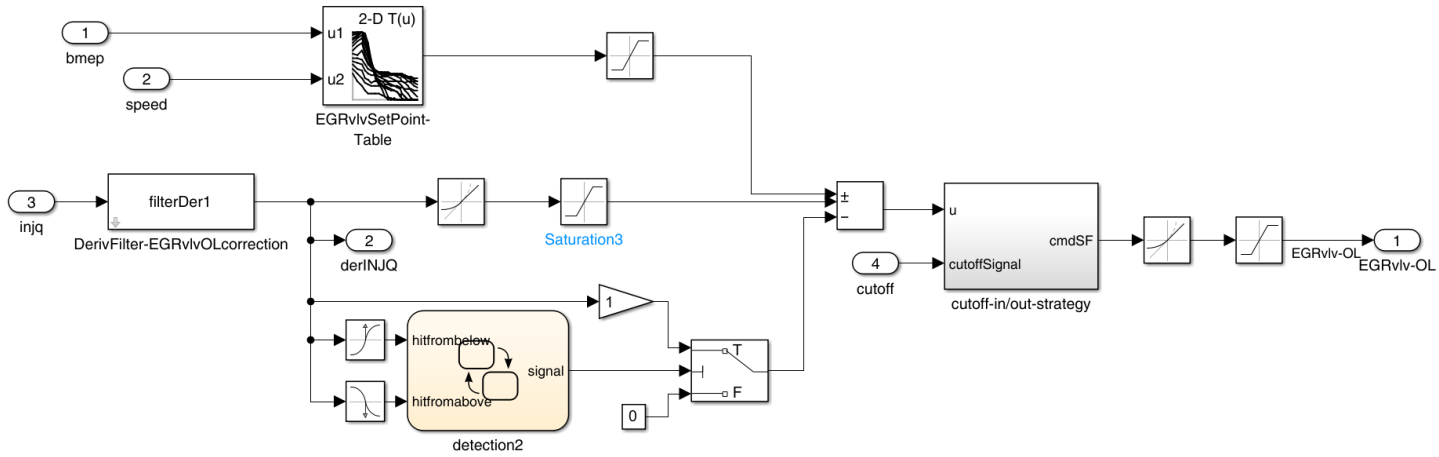


Figure B1. EGR control, open loop branch

EGR Closed loop branch

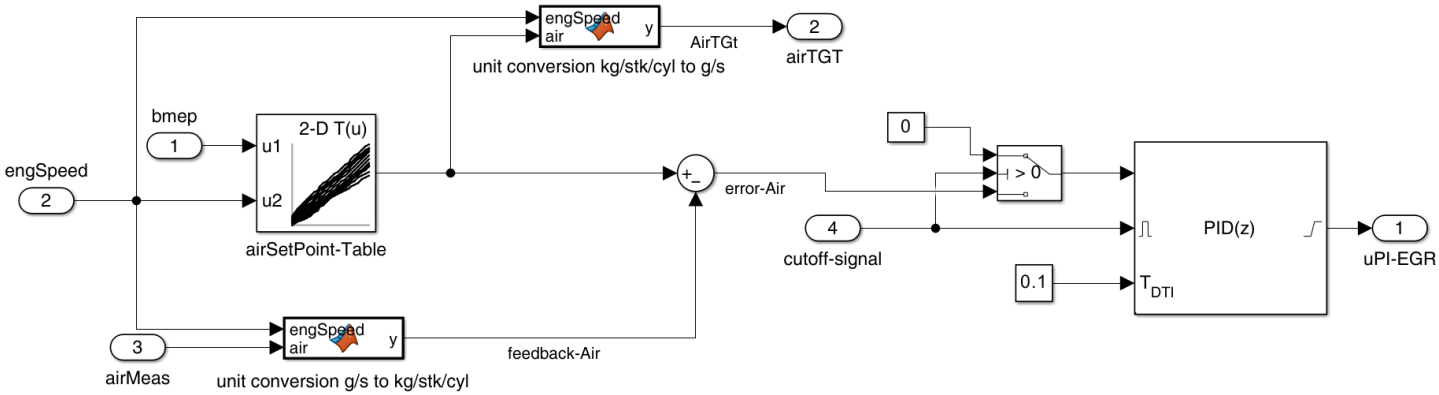


Figure B2. EGR control, closed loop branch

VGT

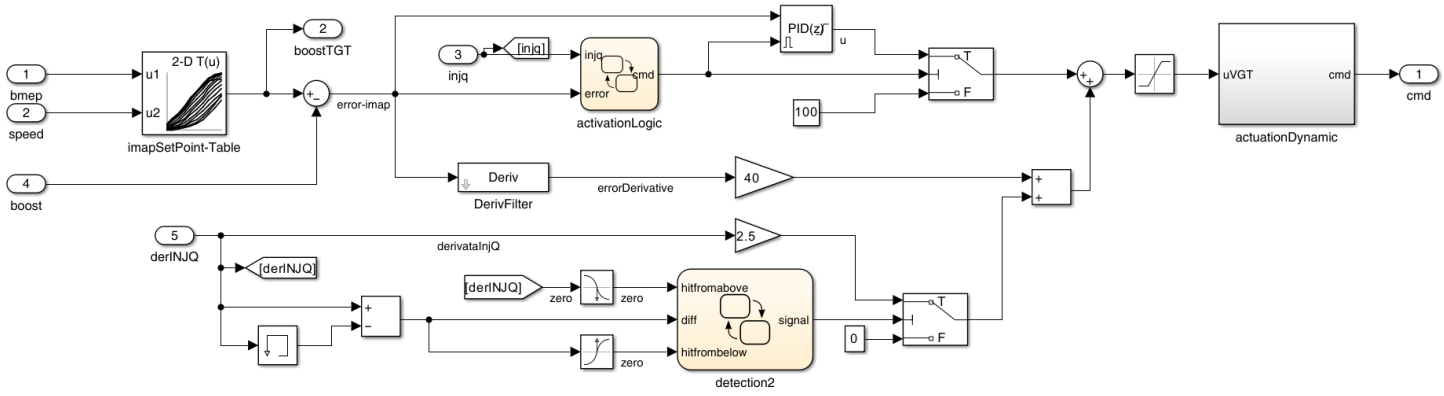


Figure B3. VGT control